Time of Failure of Metallic Nanowire Networks under Coupled Electrical and Thermal Stress: Implications for Transparent Electrodes Lifetime

Joao Resende, Dorina Papanastasiou, Dominik Moritz, Nil Fontanals, Carmen Jiménez, David Munoz-Rojas, Daniel Bellet

Time of Failure of Metallic Nanowire Networks under Coupled Electrical and Thermal Stress: Implications for Device Lifetime

Joao Resende[1,2,‡], Dorina T. Papanastasiou[1,‡], Dominik C. Moritz[1], Nil Fontanals[1], Carmen Jiménez[1], David Muñoz-Rojas[1], and Daniel Bellet[1,*]

[1]Univ. Grenoble Alpes, CNRS, Grenoble INP, LMGP, 38000, Grenoble, France

[2]AlmaScience Colab, Madan Parque, 2829-516 Caparica, Portugal

Abstract

Silver nanowire networks are extensively studied due to their excellent optical and electrical properties and exceptional flexibility. These networks constitute a promising candidate for transparent and flexible electrodes applications. However, they can degrade under electrical or thermal stresses, so the understanding of the degradation mechanism is crucial for the integration of these metallic nanostructures in devices. In the present work, the electrical resistance of about 200 silver nanowire networks was monitored *in situ* to study the failure mechanisms under constant electrical current and temperature, to assess the prevailing stress in the failure process. For both origins of failure, electrical and thermal, the temperature-induced instabilities appear to be the prevailing phenomena at the origin of the network degradation. A semi-empirical physical model is proposed considering the generated Joule heating and the effect of the imposed temperature.

This model allows to calculate the time of failure of silver nanowire networks for different electrical and thermal applied conditions and network densities, showing a good agreement with experimental data. The proposed model provides a deeper insight and constitutes a quantitative prediction tool for stability assessment, thus contributing to propel the integration of nanowire networks into devices, thanks to their robustness and reliability.

KEYWORDS: Transparent conductive materials, TCM, AgNW, stability, transparent electrode, transparent heater, Joule heating

Introduction

Transparent Electrodes (TE) are essential for a large variety of energy, lighting and heating devices, such as solar cells, liquid crystal displays (LCDs), organic light-emitting diodes (OLEDs), touch panels, gas sensors, transparent heaters, smart windows, low-emissivity coating, electrochromic devices, resistive switching devices, transparent electromagnetic interference shielding, medical devices and smart clothing [1–9]. While indium tin oxide (ITO) has so far dominated the field of transparent electrodes, ITO is becoming too costly [10] and its brittleness is a limiting factor for the current increasing demand on flexible electronic devices [11]. Metallic nanowire random networks represent a promising alternative to ITO, having shown outstanding properties in terms of low sheet resistance at high transparency combined with a high flexibility [3,12,13]. In particular, silver nanowire (AgNW) networks exhibit similar optical and electrical properties to ITO-based electrodes, namely sheet resistance values below 10 Ω/sq and optical transparency of 90% [14], while using less material per unit area [15,16]. AgNW networks are also mechanically stable under bending tests when deposited on flexible substrates [11]. Furthermore, the

deposition of these metallic networks is compatible with large area and cheap solution-based deposition techniques [17].

The enhancement of the electrical properties of AgNW networks is directly linked to a reduction of resistance of the overall network, mainly due to contact resistance between different nanowires. Therefore, the improvement of the electrical resistance can be achieved by desorption of the PVP coating on the contact point of adjacent nanowires and by the active diffusion of Ag atoms towards nanowire junctions through a local sintering process [18,19]. In the literature, the optimization of the juntion resistance between overlapped AgNWs has been highly explored using thermal and electrical treatments to the metallic network [18,20], as well as mechanical pressure [21], plasmonic welding [22] or cold welding techniques [23]. Nevertheless, if the temperature increases locally in the network, the excess of heating can compromise the conductive properties of the electrode by a thermally induced morphological destabilization of the nanowires resulting in a loss of electrical percolation.

This morphological evolution is originated from the thermodynamic Plateau-Rayleigh instability[18], as the system reduces its surface energy by changing the morphology from nanowires to nanoparticles. One of the main interest to study this instability is either to increase thermal stability or to use it as a processing route[24]. It is well-known that the first instability wavelength associated to Plateau-Rayleigh instability is the perimeter of a nanowire ($2\pi R$), when expressed in its simplest approach, as reported in textbooks or articles[25–27]. However, the instability wavelength can depend on several parameters, such as temperature or substrate topography[28]. When applied to a metallic nanowire network, this process of spheroidization results in the loss of the network percolating nature, which is associated to the divergence of the AgNW network electrical

resistance. This phenomenon has been observed in networks under high thermal stresses, for temperatures above 250 ºC, depending on the diameter of the nanowires, and affecting the entire network[29].

Nevertheless, AgNWs can also be impacted by the flow of electrical current [30,31]. When AgNW networks undergo a low electrical stress, the main observation concerns the Joule heating effect that increases the network temperature over its entire area [32]. For larger electrical stress, failure mechanism is also observed leading to the loss of electrical percolation of the network [33–35]. However, the destabilization of the nanowire morphology by spheroidization occurs locally [33,36], contrarily to the thermal degradation under thermal stress. Even though both electrical and thermal failures show the same kind of AgNW degradation at the nanoscale, driven by the same Plateau-Rayleigh instability principle, their different phenomenology yields different macroscopic network degradation processes. In other words, while thermally-induced failure will occur in nearly all nanowires of the heated network, electrically-induced failure will only have a local degradation effect of the network in the crack propagated from the hotspots.

In this study, we explore the impact of combined electrical and thermal stresses on the stability of AgNW networks by following the *in situ* evolution of the networks electrical resistance. In our study, we apply a set of current (I) and temperature (T) conditions to similar AgNW networks samples, in order to determine the Time of Failure (ToF) in each experiment. In total, nearly 200 specimens have been investigated with this approach, which is statistically representative. These results are then used in a physical semi-empirical model to obtain a predictive method for the ToF value, while considering the differences in network densities between networks reflected in initial resistance variations and current density (j) applied to each individual network. Therefore, we

obtain a semi-empirical current density-temperature (*j-T*) model dependent on the network density, capable of predicting the *ToF* of transparent and conductive AgNW networks on a glass substrate. This prediction appears of clear importance for a better understanding and design of metallic nanowire networks for an efficient integration into industrial devices.

Results and Discussion

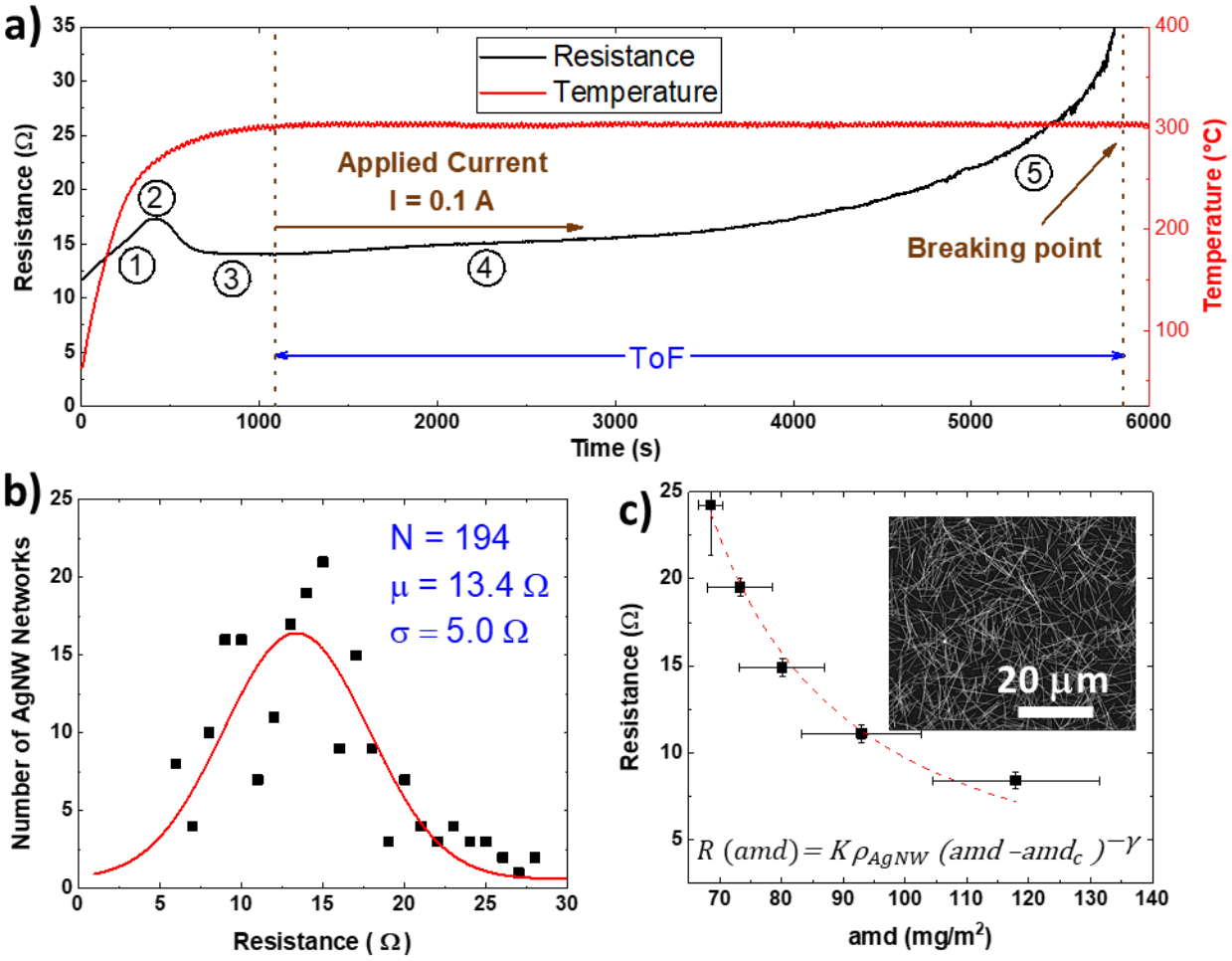

Figure 1a) shows the time evolution of the resistance during the electrical and thermal *I-T*

experiment on a sample, which was heated up to 300 °C and electrically stressed at constant current of 0.1 A.

For the sake of clarity, the term “thermal stress” and “electrical stress” have to be explained. One can define them in the following way: i) thermal stress (i.e. applying a given temperature) drastically activates the atomic diffusion (eq. (5) relates quantitatively its dependence with temperature), knowing that surface diffusion appears to play a key role for metallic nanowires; ii) electrical stress (i.e. applying an electrical voltage current) mainly accounts for the current-induced Joule heating. Conversely to thermal stress for which the temperature is spatially uniform, Joule heating could be largely non-homogeneous and local hotspots can exist in some locations and lead to AgNW network degradation (see for instance Sannicolo *et al.* [33])

The resistance evolution of

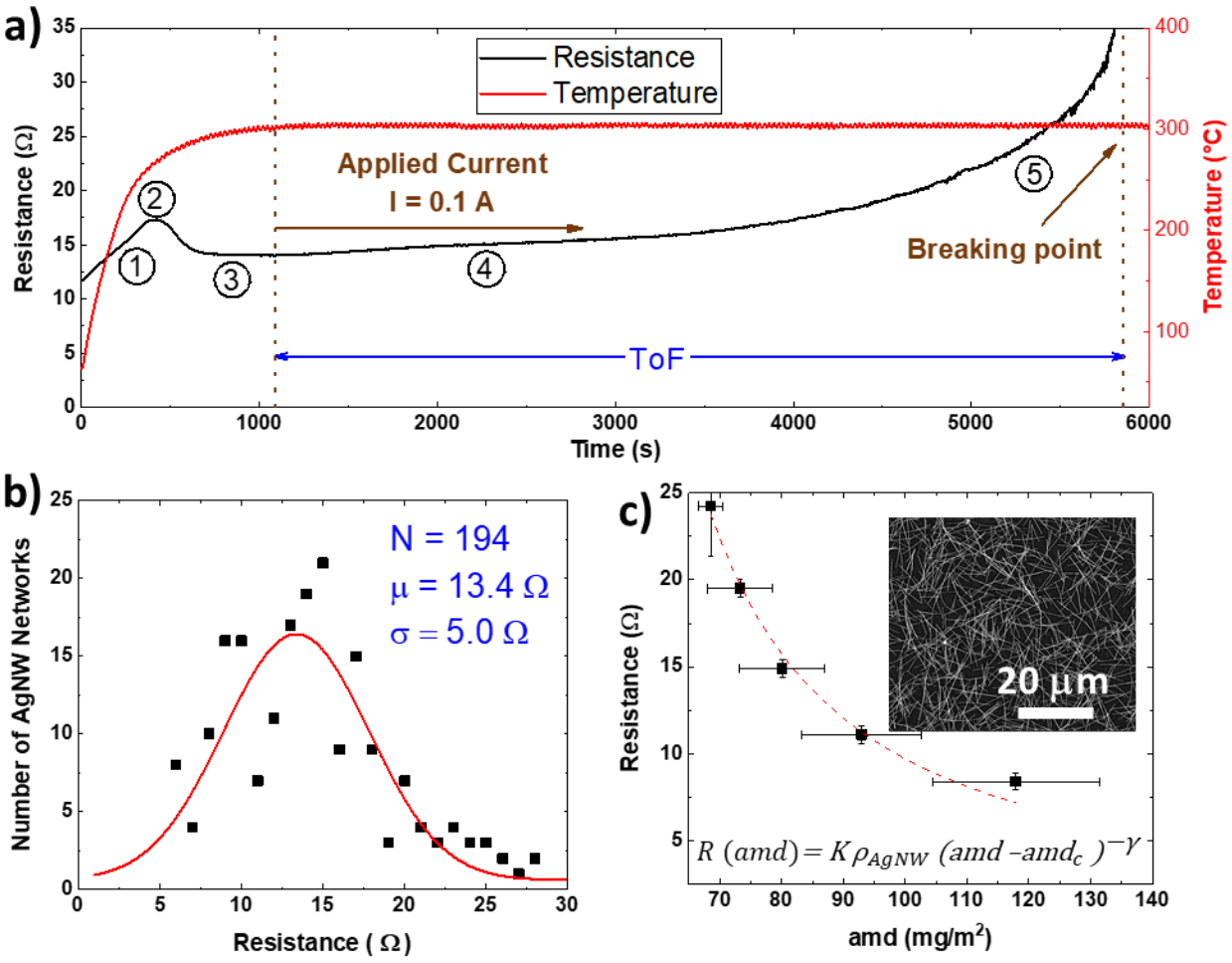

Figure 1a) can be divided into 5 different regions. Region 1 shows the linear increase of resistance, R, with increasing temperature at constant heating rate, in accordance with the metallic behavior of AgNW networks: $R(T_0 + \Delta T) = R_0(T_0)(1 + \beta\Delta T)$. From this linear relation, one can calculate the thermal coefficient for AgNW networks β_{AgNW} being 2.1x10^{-3} K^{-1}, a value close to the one reported by Lagrange et al. [14] of 2.2±0.1 x10^{-3} K^{-1}. At a temperature of around 250 °C, the resistance decreases (Region 2) because of the sintering taking place at the junctions between nanowires. The surrounding PVP layer of the nanowire exhibits a glass transition temperature of 174 °C and a melting point at 220 °C [21]. The PVP layer degradation increases the contact area of

the junctions and leads to an improvement of the overall conductivity of the network. When the applied temperature stabilized, in this example at 300 °C, the resistance showed almost no further decrease, as observed in Region 3. At this steady state temperature, the current corresponding to the examined *I-T* couple, here 0.1 A, started to be applied. In this method, the current is applied and *ToF* is counted starting from the point at which a steady temperature is reached. The choice of a rather high temperature rate (15 °C/min), larger than usual (see Lagrange *et al.* [14] or Bardet *et al.* [37], where thermal ramps of 2 and 5 °C/ min, respectively, were used) was considered in order to minimize the morphological instability during the thermal ramp. The electrical power during the current flow is dissipated by Joule heating in the AgNW network and is expressed as $P_{in} = I^2 R$. According to Sorel et al. [32] the increase of temperature of a AgNW network due to Joule heating can be approximated as:

$$T(t) \approx T_0 + \frac{I^2 R}{\alpha A}[1 - e^{-t/\tau}] \quad \textbf{(1)}$$

$$T_{stab} = T_0 + \left(\frac{I^2 R}{\alpha A}\right) \text{ for steady-state temperature} \quad \textbf{(2)}$$

where α and τ are referred as heat and time constant, respectively, and $\frac{I^2 R}{A}$ stands for the areal power density, while A is the specimen area, and T_0 is the applied macroscopic temperature. This increase of temperature is concomitant to the temperature imposed on the sample through the hot-plate and leads to a thermalization of the sample by compensating the heating power. On a closer examination at Region 4, a limited increase in resistance can be observed. Therefore, in these conditions there is no steady state visible; instead there is a smooth continuity between Region 4 and 5, without any abrupt change. Region 5 describes the non-reversible degradation of the network with a sharp increase of the electrical resistance, which rapidly leads to the failure point.

In this *I-T* experiment, 194 specimens of random silver nanowire networks were produced, which exhibit a dispersion in terms of electrical resistance. The initial resistance values of the whole set of samples follow a Gaussian distribution (see the red curve in

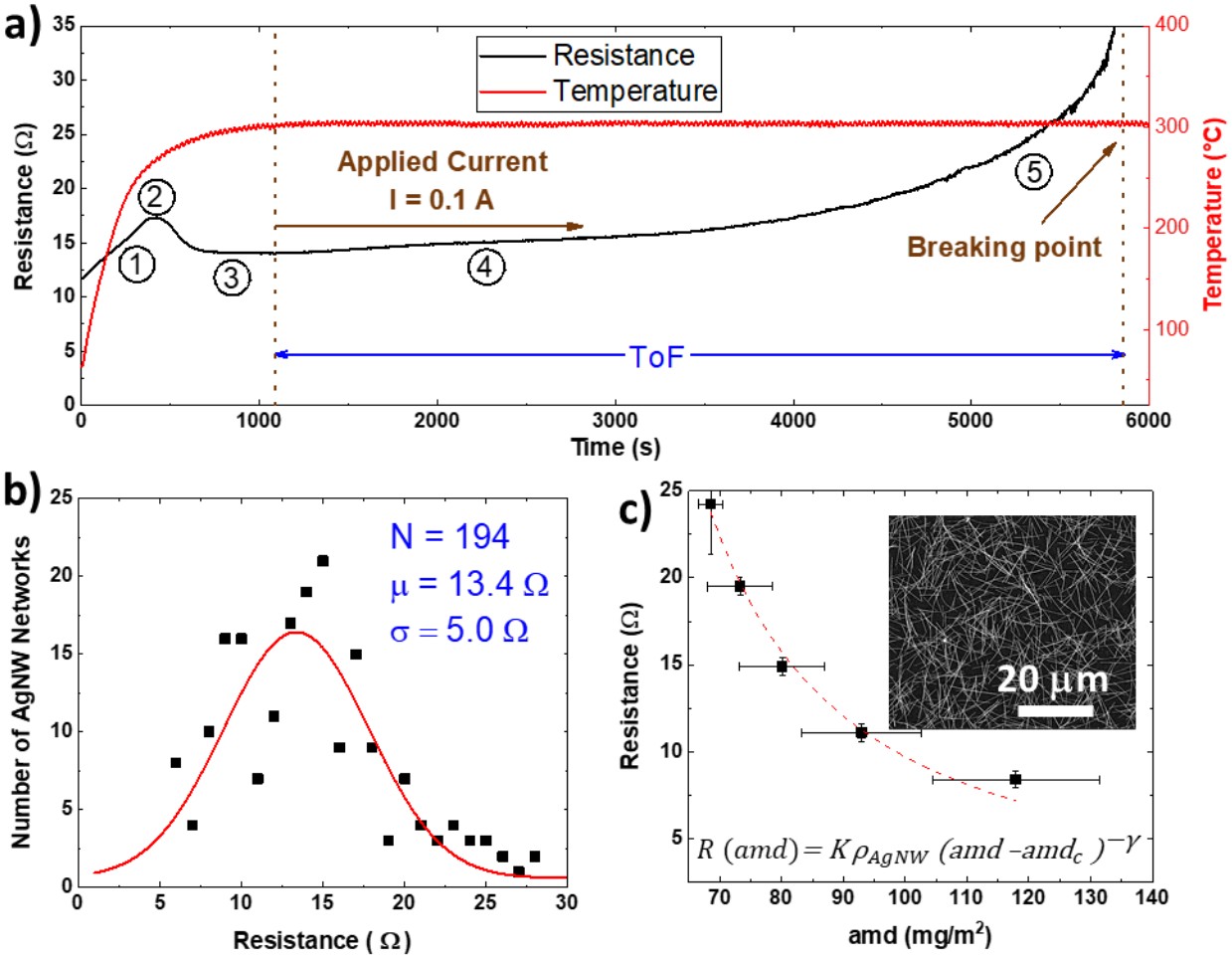

Figure 1b), with an average resistance (μ) of 13.4 Ω and a standard deviation (σ) of 5 Ω, as reported in

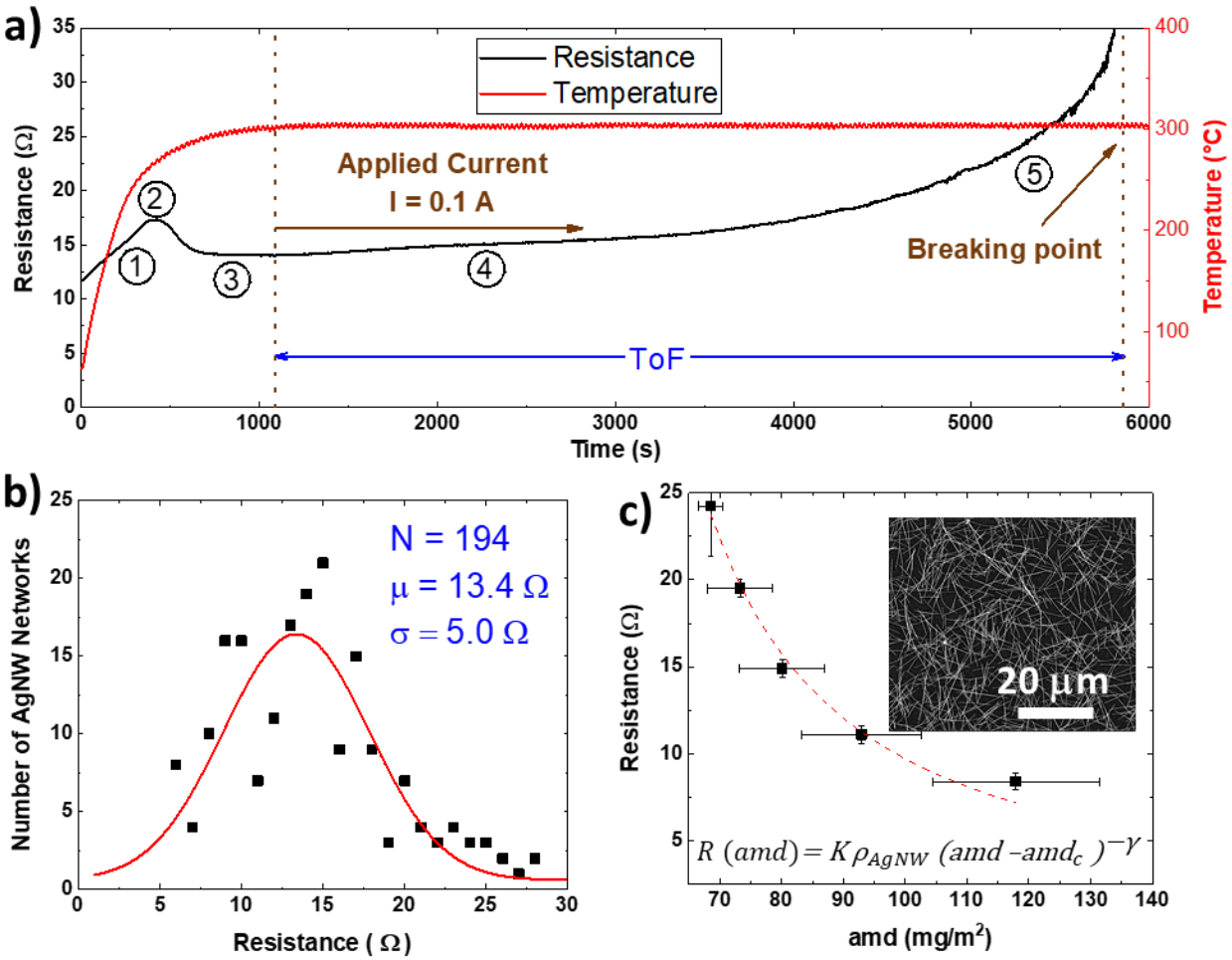

Figure 1b). This resistance distribution, ranging from 5 to 28 Ω, originates from the variations of the areal mass density (*amd*) during the deposition of the AgNW networks. SEM observations reveal that the *amd* varies indeed from 70 mg/m^2 up to 120 mg/m^2 in this group of random networks. The electrical resistance has a power-law dependence with the network density [14]:

$$R\ (amd) = K\ \rho_{AgNW}^{el}\ (amd - amd_c\ )^{-\gamma} \qquad \textbf{(3)}$$

where the resistance is proportional to $(amd - amd_c\ )^{-\gamma}$ for which amd_c is the critical density of the network for percolation of 39 ± 3 mg/m^2 and γ is a proportionality factor between 1.23 and 1.43 [38], considered here as 1.33. K is a specimen shape parameter fitted as (1.0 ± 0.1) x 10^9 mg$^{4/3}$.m^{-}

[11/3] and ρ_{AgNW}^{el} is the electrical resistivity of one single silver nanowire, considered to be 2.0 x10^{-6} Ω.cm for a AgNW with a diameter of 79 nm. Moreover, the network resistance is considered in series with an instrumental set-up resistance of 1 Ω, as previously reported by Lagrange et al. [14]. The experimental variation of network resistance with the areal mass density is represented in

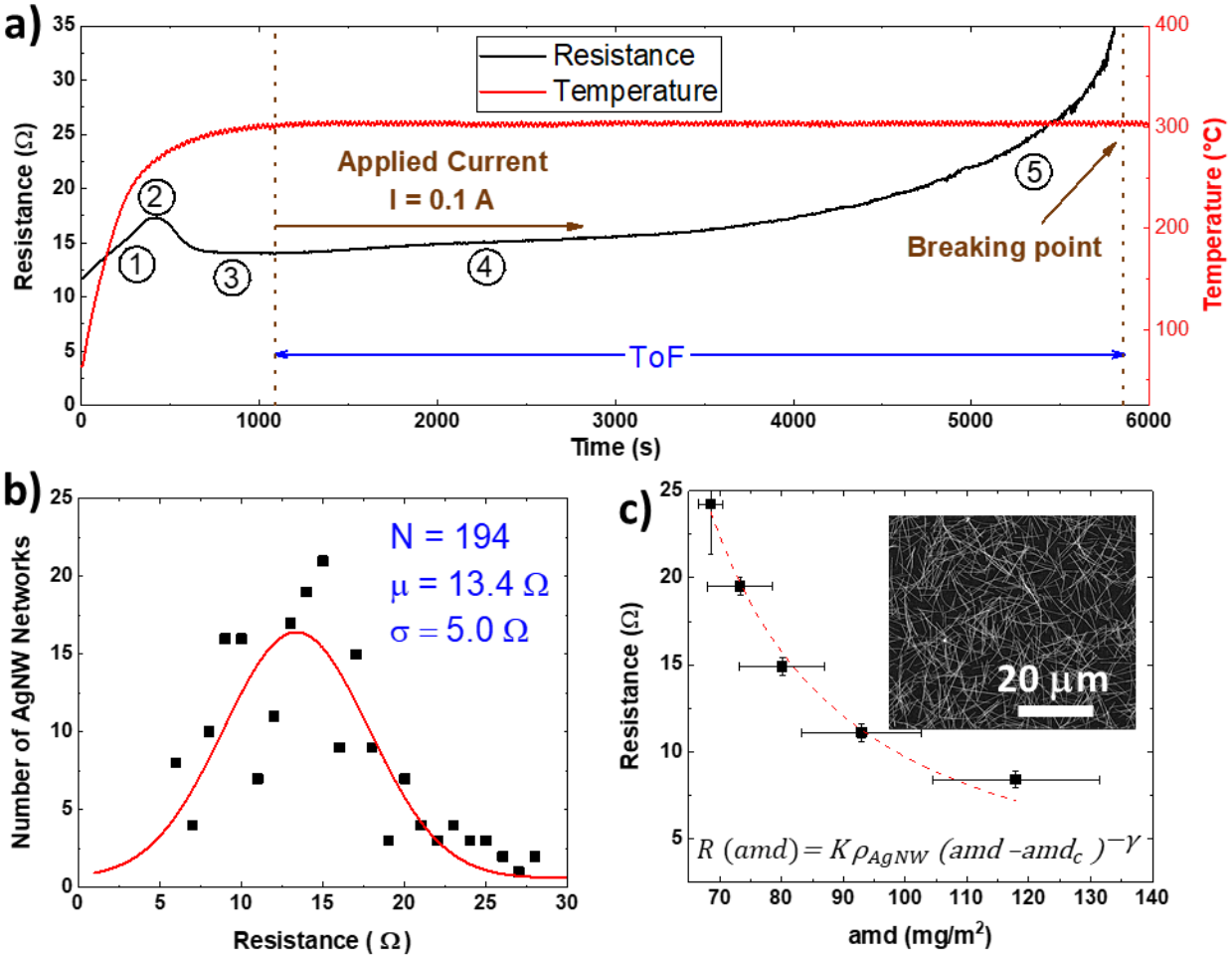

Figure 1c) together with the dependence obtained by applying Equation (3): a fair agreement is obtained. A SEM picture corresponding to a network with *amd* of 73 ± 5 mg/m^2 is shown in the inset.

The *ToF* of this set of AgNW networks was determined while having into consideration three different parameters: the network initial resistance, the applied electrical current and the applied temperature.

Initial network resistance influence

The dependence of ToF with the network initial resistance was ensured on samples having different initial electrical resistances by performing the measurements using the same applied temperature and electrical current values. In Figure 2a), the evolution with time of the electrical resistance during the I-T experiment is plotted for AgNW networks with initial resistances of 10.5, 12.4 and 17.4 Ω heated at 150 °C and applying a current of 0.5 A. As shown in Figure 2a), the ToF drastically depends on the initial resistance. This is a general trend of the I-T experiment: the higher the initial electrical resistance, the shorter the ToF. This result is directly related to the areal power density, presented in Equation (2): a higher resistance leads to a higher areal power density, which increases the temperature of the specimen. Therefore, the sample degrades faster and the ToF is indeed shorter. While a given AgNW network is characterized by its electrical resistance at the macroscopic level, locally it exhibits some areas with different network density that can lead to different percolation pathways as demonstrated by Sannicolo *et al*.[39] This can eventually give rise to hotspots that can locally increase the temperature significantly so as to destabilize the networks, triggering the formation of electrical cracks that lead to the electrode failure[33].

Influence of applied temperature

To observe the influence of temperature, AgNW networks with similar resistance values of 16.0 ± 0.9 Ω, were chosen along with a constant current 0.25 A. Data associated to the *ToF* determination

for temperatures from 175 to 300 °C are shown in Figure 2b). As expected, the increase of the applied temperature, thus the thermal stress, leads to a faster failure. For instance, for temperature lower than 200 °C, the samples are stable for more than 24 hours, while for temperatures above 300 °C the electrical breakdown is very fast, occurring in less than 10 minutes. This can be easily explained since increasing temperature leads to a much more efficient atomic diffusion, which promotes the kinetics of Plateau-Rayleigh instability and therefore lowers *ToF* [18].

Influence of electrical current

A similar study was performed by applying different electrical current values. A group of AgNW networks having an initial resistance of 15.5 ± 0.3 Ω were selected and the temperature was set to 225 °C. As shown in Figure 2c), as expected, the higher the current applied on AgNW networks, the shorter the *ToF*. For instance AgNW networks remain stable for more than 8 hours under a low applied current of 0.1 A. On the other hand, at higher electrical current of 0.25 A, the time of failure is much shorter, less than 15 minutes. At even higher values of current, of 0.5 A, we observe an almost instant divergence of the electrical resistance. This behavior can also be associated to the areal power density, as the increase of current results in a higher areal power density and increase of local induced temperature for the AgNW networks (see Equation (2)).

Towards Predicting the Time of Failure model

In order to obtain a deeper quantitative insight into the role played by these parameters, a physical model is proposed. The experimental approach exposed previously can be used to assess a physical and semi-empirical model that can predict the *ToF* of AgNW networks in under given conditions.

The proposed model should be based, in the most pertinent way, on mechanisms of failure associated to the induced stresses.

The thermal approach, where atomic diffusion operates over a characteristic distance, L_{therm}, allowing the AgNW morphological instability occurrence, can be described by the following classical equations from atomic diffusion [40]:

$$L_{therm} = \sqrt{2\ D\ t_{therm}} \tag{4}$$

$$\text{and } D = D_0\ exp(-\frac{E}{k_B T}) \tag{5}$$

where D is the diffusion coefficient and t_{therm} is the characteristic thermal time, D_0 and E are the pre-exponential factor and a thermal activation energy, respectively. These parameters concern only the thermal stress. One can combine both Equation (4) and Equation (5) to estimate *ToF* when solely thermal stress is applied; in such conditions *ToF* can be noted t_{therm}:

$$t_{therm} = \frac{{L_{therm}}^2}{2D_0} exp\left(\frac{E}{k_B T}\right) = B\ exp\left(\frac{E}{k_B T}\right) \tag{6}$$

with parameter B depending on the nanowires features such as their dimensions.

For the electrical stress, it appears more pertinent to consider a local analysis, replacing then the applied current, I, by the current density, j. This has two main advantages: i) the analysis is independent on the network dimension, therefore comparison with data from literature is more straightforward and ii) comparison between failure at the network scale, as in this work, and the AgNW scale, as presented in literature can also be directly achieved. In Supporting Information, the geometrical considerations are described to establish a cross-section area (*CS*) dependence with

the network *amd*. The resulting formula can be expressed for a square network of length L (i.e. distance between opposite electrodes) as:

$$CS = \frac{L\ \pi\ {D_{AgNW}}^2}{4\ \mathrm{l}} = \frac{L\ \ amd}{2\ \rho_{Ag}^{m}} \qquad \textbf{(7)}$$

where D_{AgNW} is the average diameter of AgNWs.

Thus, the applied current can be replaced with the corresponding current density, $j = \frac{I}{CS}$, in order to obtain a relation for the current density j versus the applied current I and the network density, *amd*:

$$j = \frac{2\ I\ \rho_{Ag}^{m}}{L\ amd} \qquad \textbf{(8)}$$

Equation (8) enables to calculate current density values associated to this work: an electrical current I of 0.5 A, an *amd* of 100 mg/m^2, L=12.5 mm, then the current density is equal to 0.84 10^{10} A/m^2 or sometimes as well expressed as 0.84 MA/cm^2. This value is coherent with values found in literature; Charvin et al. have reported a current density of failure equal to 1.63 MA/cm^2 [36], and Lagrange et al. equal to 3.1 MA/cm^2 at 7.5 V[41]. In addition, Khaligh et al. have estimated by simulations that AgNW networks can be stable when carrying an average current density of 0.12 MA/cm^2 [42]. All these electrical current density values associated to network failure are of the same order of magnitude considering that the applied stress is different and AgNW have different characteristics, such as dimensions and surface chemistry. Therefore, due to the conversion of applied current to applied current density, one can consider all studied AgNW networks and then take into account their own electrical resistance value.

The *ToF*, plotted in log scale, for all the networks studied as a function of temperature and applied current density is shown in Figure 3. The relation between log (*ToF*) and the reciprocal temperature is depicted in Figure 3a), with a color map representing the current density. In Figure 3b), the *ToF* is presented as a function of the current density, with a color map showing the applied temperature for each AgNW network. It is clearly visible that in the extreme case of high current density, i.e. 1.5 MA/cm^2, the AgNW networks degrade very rapidly, with a corresponding *ToF* lower than 100 seconds, even when exposed to temperatures below 150 ºC. Inversely, close to zero electrical current density, the failure occurs mainly for the samples that undergo applied temperatures over 300 ºC. The intermediate cases of 0.5 to 1 MA/cm^2, the *ToF* shows large variation values. In this region, the *ToF* values demonstrate an entanglement of both electrical and thermal stress. However, observing the evolution of *ToF* for the same current density, we can notice a general trend of a decrease of the *ToF* as the temperature increases.

The generalization for both thermal and electrical stresses can be accomplished using the steady state temperature Equation (2), which considers that the applying electrical bias induces a local temperature increase, due to Joule heating. So, for the calculation of the *ToF*, during both electrical and thermal stress, the temperature T can be replaced by $T_0 + \Delta T$, where ΔT corresponds to the temperature increase induced by Joule heating. Then Equation (6), which associates the *ToF* solely to the thermal stress, can be in a first approximation used by considering the temperature given by Equation (2). Then, the time of failure *ToF* can be written as:

$$ToF = B\ exp\left(\frac{E}{k_B\ (T + \Delta T_{local})}\right) \quad \textbf{(9)}$$

where E is an activation energy, T is the applied temperature and ΔT_{local} is the temperature increase induced by Joule heating. This local temperature approach is valid at the macroscopic level. As already mentioned, the goal is to obtain an expression of *ToF* restricted to the local level. Instead of considering macroscopic parameters, such as the electrical resistance and the current, one can consider the local parameters as the *amd* and the electrical current density. This allows introducing the local physical mechanisms. The relation between electrical resistance R and network density *amd* is represented in Equation (3), while the dependence between current I and current density j is simply shown as $I=j.CS$. Therefore, the local increase of temperature, ΔT_{local}, can be written in a way equivalent to the areal power density, locally equal to ρ^{el}j² with ρ^{el} the electrical resistivity of AgNWs, which follows a macroscopic perspective. For a local perspective one can obtain:

$$\Delta T_{local} = \frac{areal\ power}{\alpha^{local}} = \frac{(\rho^{el}\ j^2)\ \left(V_T^{\ AgNWs}\right)}{\alpha^{local}\ A} \tag{10}$$

where α^{local} is the local heat transfer constant, $V_T^{\ AgNWs}$ is the total volume of AgNWs in the whole network and A is the network geometric area, equal to L^2. The term $V_T^{\ AgNWs}$ can be estimated from the total mass of silver within AgNW network, $M_T^{\ AgNWs}$ given by :

$$M_T^{\ AgNWs} = \rho_{Ag}^{m}\ V_T^{\ AgNWs} = amd\ A \tag{11}$$

where ρ_{Ag}^{m} is the silver bulk density, 10.49 g/cm^3. Introducing the expression of the total volume of AgNWs from Equation (11) into Equation (10), results in an expression for the local increase of temperature:

$$\Delta T_{local} = \frac{\rho^{el}\, j^2\, amd}{\alpha^{local}\, \rho_{Ag}^{m}} = C\, j^2\, amd \qquad (12)$$

where C is a constant equal to $\frac{\rho^{el}}{\alpha^{local}\, \rho_{Ag}^{m}}$. Equation (12) is easily explained as the local temperature increase, ΔT_{local}, should linearly increase with ρ^{el}, j^2 and *amd*. Consequently, this model provides a way to write the *ToF* of AgNW network depending on the applied conditions, temperature T and current density j, as well as the network *amd*, as follows:

$$ToF = B\, exp\left(\frac{E}{k_B\left(T+\frac{\rho^{el}\, j^2\, amd}{\alpha^{local}\, \rho_{Ag}^{m}}\right)}\right) \text{ or } ToF = B\, exp\left(\frac{E}{k_B\,(T+C\, j^2\, amd)}\right) \qquad (13)$$

This last equation possesses only three unknown parameters: B (nanowires features parameter), E (activation energy) and α^{local} (local heat transfer constant). Before comparing experimental data with the *ToF* Equation (13), one should keep in mind the limitations of the model associated to several hypotheses:

i) we first assume that the *ToF* can be expressed in an equivalent form to Equation (6). We consider that the surface atomic diffusion, triggering the nanowires morphology change, from wire shape to spheres, can be activated either by applied temperature and/or by Joule effect. The associated driving force for this process (Plateau-Rayleigh instability) is the reduction of the total surface energy;

ii) we consider that AgNW networks are homogeneous, i.e. identical *amd* throughout the whole sample, leading to a direct I to j relation, which resembles the approaches considered in the framework of mean field theory. According to this, in a stochastic model, the effect of all other

entities on any given entity is approximated by a single averaged effect. Consequently, we reduce a many-body problem into a one-body problem;

iii) we assume that all AgNWs in the network have identical diameter, and therefore identical electrical resistivity ρ^{el} since the latter depends upon AgNW diameter [43], which is in our case $\rho^{el} = 2.0$ x10^{-6} Ω.cm for D_{AgNW} equal to 79 nm. However, every AgNW solution, and as consequence every AgNW network, presents a diameter distribution [44,45].

iv) we disregard other possible degradation factors reported for AgNW networks, such as chemically induced instabilities and high humidity conditions.

Hence, the model proposed in the present work aims to provide the main tendencies in terms of dependence of *ToF* of AgNW networks with *amd*, current density and temperature. The model aims as well to predict, in a first approximation, the prevailing mechanism responsible for the degradation of AgNW networks. This can be helpful to disentangle the electrical and the thermal mechanisms of failure. The result of the modelling is presented in Figure 4, in an applied current density-applied temperature diagram, where the rainbow color map corresponds to the range of the *ToF* in log scale. The experimental values of *ToF* represented in Figure 4 for a comparison with the model were determined for samples with an average initial resistance of 13.4 Ω (*amd* equal to 86 mg/m^2).

As previously commented, the three unknown parameters are: B, E and α^{local}. The activation energy E was extracted from the Arrhenius plot, i.e. log (*ToF)* vs (1/T) when no current is applied. The value used in the model is 1.1 ± 0.1 eV, close to those observed in previous works during thermal annealing experiments, ranging from 0.3 to 1 eV [46]. In addition, the model provides the

parameter C equal to (1.97 ± 0.1) x10^{-14} K.A^{-2}.m^6.kg^{-1}, thus, the heat constant α^{local} can be calculated as (96 ± 5) W.m^{-2}.K^{-1} from $C = \frac{\rho^{el}}{\alpha^{local}\,\rho_{Ag}^{m}}$. This value is also in the same range than those of other metallic nanostructures, and graphene or carbon nanotubes, i.e. from 15 to 123 W.m^{-2}.K^{-1}, as summarized by Sorel et al. [32]. The parameter B is estimated as (5.5± 0.1) x10^{-8} s. To validate this value, B can be introduced in Equation (4) and Equation (5) to determine L_{therm}, the characteristic distance over which the atomic diffusion operates to induce the degradation of the AgNW network. The physical meaning of this characteristic distance, L_{therm}, is the following: since surface diffusion plays a key role for nanowires, in order to promote AgNW morphological instabilities, Ag atoms diffuse along the AgNW. The simplest approach to perform calculations, is to consider for L_{therm} the smallest wavelength of the cylinder perturbations that generates Plateau-Rayleigh instability. This distance corresponds to the cylinder perimeter $2\pi R$ [25]. In other words it is supposed, for the sake of simplicity, that Ag atoms should diffuse along the AgNW surface over a length associated to the AgNW diameter in order to initiate AgNW instability.

Therefore, B can be estimated as:

$$B = \frac{\pi^2 D_{NW}^2}{2D_0} \qquad (14)$$

Since B and D_{NW} are known, one can estimate the value for the pre-factor D_0: 4.4 x10^{-7} m^2.s^{-1}. This pre-factor diffusion D_0 can be compared to the atomic surface diffusion on silver (100) crystallographic planes which was estimated, for large surfaces, by Jamnig et al. as 3.7 x10^{-7} m^2.s^{-1} [47]. Although the geometry is different between silver bulk planar (100) surfaces and the surfaces of a AgNW, these two values are rather close. The three parameters determined in the *j-T* model

(E, α^{local} and D_0) for silver nanowire networks are summarized in Table 1 with a relative comparison with the reported values in the literature.

Figure 4 enables to compare in the *j-T* diagram the values resulting from the proposed model (background color) with the experimental measurements (circles). The comparison of the different *ToF* shows a rather good agreement for all stress conditions, at least from a qualitative point of view. A strict quantitative analysis is difficult to propose since the *ToF* values span over a range of several order of magnitudes: from few seconds for the extreme conditions (high temperature and/or high current density) to a few days (i.e. > 10^5 seconds). Moreover, the main goal of the proposed model was to introduce physical requirements that would be summarized in a simple formula. This simplified approach would be associated to a very small number of fitting parameters, applied for low and high temperature and current density. For such conditions, a graphical comparison with a color code was chosen and an overall good agreement between the experimental data and the model was obtained in spite of the simplicity of the model. At first glance, 3 different regimes are revealed by the semi-empirical model. The first two concern extreme cases with either instant or long *ToF*, represented by the red and blue regions, respectively. In the first case, the electrical and thermal stress have both high values (red area), i.e. in a range of 250-400 °C and 0.75-2 MA/cm^2. Inversely, when the stress is moderate, represented in the blue region, i.e. current density below 0.75 MA/cm^2 and temperature below 250 °C, it can take several days for the AgNW networks to degrade. Between these two extremes, there is a rainbow region, with a continuous increase of the *ToF*, indicating an entangled contribution of both electrical and thermal stress. This is less prominent for temperatures below 100 °C, where the increase of *ToF* seems independent of the thermal stress and almost linear, in logarithmic scale, with the electrical

one. Above this temperature threshold, it becomes harder to distinguish which mechanism of failure is dominant.

We present in Figure 5 the safe working conditions and the general regimes of degradation after electrical and thermal stress, in order to complement the *j-T* model. The three main regimes of degradation are directly associated to 3 regions in the *j-T* diagram: a) the electrical stress is solely involved and the impact of temperature is negligible, b) the thermal and the electrical stresses play a key role, and c) the thermal stress is dominant for applied temperatures over 300 °C as the low or almost zero current density is induced. The SEM images corresponding to these degradation regimes are included in Figure 5. In the first case of electrical stress, AgNW networks appear intact over the whole network area except from the regions where the crack has propagated [36]. Such highly localized regions contain damaged nanowires, partially or fully spheroidized, like the ones shown in Figure 5a), which is associated to the electrical degradation. In the intermediate case, where both the applied temperature and current are significant, the SEM images in Figure 5b) reveal similar damages observable in the overall AgNW network, with a fragmentation of silver nanowires. Finally in the case where the thermal stress dominates, SEM images, like Figure 5c), confirm the complete spheroidization of AgNW over the whole network, as previously observed during thermal annealing studies [18]. Moreover, it is worth mentioning that the "safe" area for appropriate working conditions of a device corresponds to the green zone, for which current density and temperature are typically lower than 0.5 MA/cm² and 150 °C, respectively.

The degradation of the AgNW network appears thermally activated from both high applied temperatures and the electrically induced Joule heating. Other studies concerning the current flow, usually attribute the failure not only to Joule heating but also to electromigration, inspired by

microelectronics and the Black's mean *ToF* for semiconductor circuits [34,48]. However, the scale of the macroscopic physical approach related to AgNW networks is different from the scale of individual nanowires, and therefore a direct comparison cannot be achieved [49]. Only for conditions of low electrical bias and temperatures, previous studies reported a fit of the data with the Black's equation [34]. In our case, we observed by experiments and simulation that the degradation is mainly driven by thermally induced morphological instabilities, either directly related to high imposed temperatures (Plateau-Rayleigh) or indirectly by the power-induced heating (local high current density). This approach combined the electrical and thermal contribution to the thermally activated atomic diffusion, in order to calculate the *ToF*. Thanks to its rather good agreement with experimental values, as shown by Figure 4, and the prediction of physical constants, summarized in Table 1, this *j-T* model can be used to estimate the lifetime of AgNW networks based devices where a significant electrical or thermal stress is applied.

While the calculated *ToF* values reported in Figure 4 correspond to a network density of 86 mg/m^2 and AgNW average diameter and length of 79 nm and 7 µm, respectively, the model can easily consider other *amd* values or AgNW dimensions, as well as, other metallic nanowire networks, such as copper nanowires. For instance, increasing *amd* value will correspond to larger *ToF* values, as this will reduce the current density applied. Decreasing AgNW diameter will decrease *ToF* for a faster degradation, since the parameter B in Equation (14) will also decrease; moreover the reduction of D_{NW} leads also to an easier spheroidization of AgNW due to thermodynamic arguments [14]. Finally, while the present work is focused on bare AgNW networks, a similar approach could also be applied on coated AgNW, which exhibit enhanced thermal and electrical stability [11,50] thanks to the presence of thin oxide layers. To deposit in a conformal way the latter, spatial atomic layer deposition can be employed, which is a vacuum-free and scalable technique

[51], therefore compatible with high throughput AgNW networks production such as roll-to-roll technology.

Conclusions

The stability under electrical and/or thermal stress is crucial for the performance and integration of AgNW networks into devices for many applications. Nearly 200 AgNW networks, with different initial electrical resistances, were investigated by measuring *in situ* the evolution of the resistance for an applied current and a given temperature. The increase of the resistance above a critical usage was used to determine their *ToF*, under thermal and electrical stresses. Consequently, we obtained statistically relevant data, showing the prevailing tendencies for both electrical and thermal stresses. The influence of initial network resistance, applied electrical current and temperature was thoroughly analyzed. Our results show the presence of three different regions in the obtained *j-T* diagram: two extreme cases of high and moderate stress, and a region where both thermal and electrical stresses exhibit both significant effects. In the extreme cases, the failure can be either ultra-fast or take several days, while in the intermediate cases it is rather hard to distinguish which stress is the prevailing failure mechanism among thermal and electrical stress.

A semi-empirical model is proposed to estimate the *ToF* of a network for given conditions of electrical bias and/or temperature, as well as different network areal mass density. The model is based on the physical idea that the temperature associated to the diffusion mechanisms can be considered as the applied temperature at the origin of the Plateau-Rayleigh instability, plus an additional term which stems from the power-induced Joule heating, associated to the local high current density.

The good agreement between calculated and experimentally observed *ToF* values indeed shows that this physical hypothesis appears relevant, as the degradation of the metallic network is grounded on a thermally activated phenomenon. The proposed model provides a useful tool for estimating the lifetime of AgNW networks when subjected to electrical and thermal stress. Therefore, the present approach, although semi-empirical, can be used for any metallic nanowire networks and it can have an important impact to propel the integration of metallic nanowire networks in industrial devices thanks to an optimized design of the network.

Experimental Methods

Deposition of AgNW networks

Silver nanowires were kindly provided by the research team of Jean-Pierre Simonato from CEA-LETI, France; the synthesis of these AgNWs is detailed in Mayousse et al. [52]. AgNWs exhibit an average diameter of 79 ± 10 nm and an average length of 7 ± 3 µm. The AgNW dispersion was prepared with a concentration of 0.1 g/L in methanol. An alkaline 12.5×12.5 mm^2 earth boroaluminosilicate glass (Corning 1737) was used as substrate. Glass cleaning consisted in sonication during 15 minutes in isopropanol, rinsing with distilled water, and finally drying with N_2 gas. The fabrication of the AgNW networks was conducted via spray deposition using a home-made airbrush set-up composed of a spray gun, a robotic arm and a heating plate. N_2 was used as spraying gas with a pressure of 1.4 bar. Substrates were heated at 110 °C to easily evaporate the solvent and to avoid coffee rings formation. The network density was controlled by adjusting the number of spray cycles, and measured after network fabrication thanks to scanning electron

microscopy (SEM). Silver-paste-based contacts were manually deposited at two opposite sides of the square specimen and dried for 12 hours in the ambient air.

Characterization techniques

Scanning Electron Microscopy (SEM) was conducted in a FEI Quanta 250 FEG-ESEM tool. The areal mass density (*amd*), which corresponds to the mass of material per unit surface, was estimated using SEM micrographs with the same area size and a plugin of the Software *ImageJ*.

Endurance test under thermal and electrical stresses

The electrical and thermal endurance tests were performed in a home-made set-up including a hot plate with a Proportional Integral Derivative (PID) controlled system and a thermocouple and two pairs of two-point probes. These two pairs of two-point probes were used to measure simultaneously two different samples under the same experimental conditions. The heating parameters were controlled by a National Instruments™ input module thanks to a LabVIEW software that controls and records every second voltage, current, resistance and temperature. The electrical characteristics were obtained via a Keithley 2400 sourcemeter. The measurements took place in open air and a low current of 5 mA was applied to measure the electrical resistance, such a low value leads to a negligible electrical impact on the network. The current values applied were 0, 0.1, 0.25, 0.5 and 0.75 A. The temperature was varied from 50 to 400 °C, with an increasing step value of 25 °C. The heating rate was of 15 °C/min in all the experiments to rapidly increase the temperature of the sample without compromising the mechanical stability of the glass substrate. The protocol followed for each *I-T* couple of data points was to apply a constant current only once the temperature reached the steady-state value, and then until the network resistance

reached 5 kΩ.

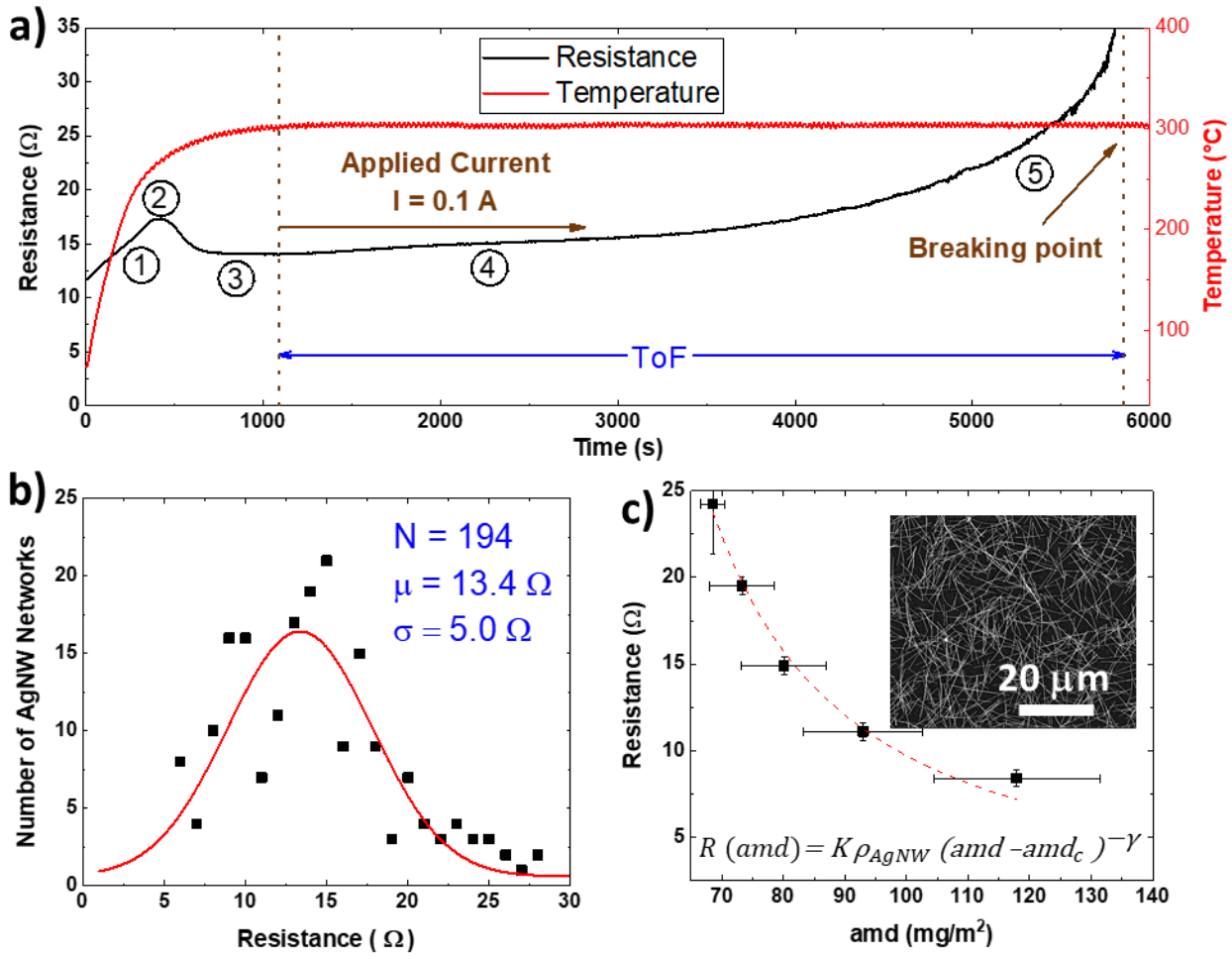

Figure 1a) shows the successive steps of the *I-T* experiment. The stabilization time ranged between 5 and 10 minutes after the beginning of the heat up stage. The moment when the target current is applied is considered as "zero" time of the experiment, i.e. when both temperature and current are imposed on the sample. At the moment that the network resistance reaches 5 kΩ, i.e. about 400 times larger than the initial resistance, the duration is defined as Time of Failure (*ToF*). The value of 5 kΩ was selected since it corresponds to a state where the AgNW networks have been degraded already enough to alter seriously any device usage for the great majority of applications.

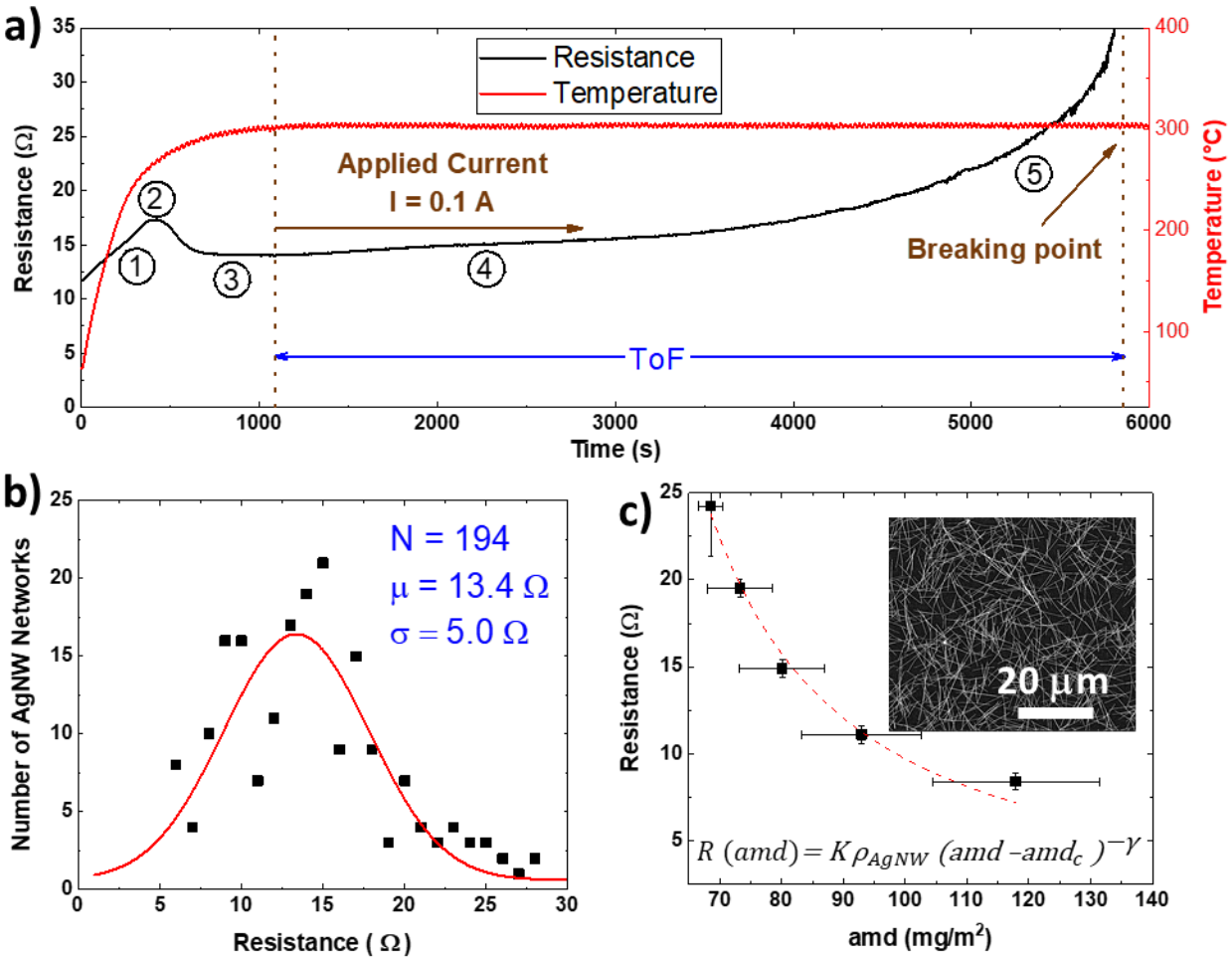

Figure 1. a) Example of a time evolution for the resistance (black curve) of a AgNW network during I-T experiment, for which a temperature of 300 ºC is applied (red curve), followed by application of an electrical current of 0.1 A. Five different steps can be observed for the time dependence of the electrical resistance (see text for description); **b)** Statistical distribution of the initial resistance, 1 Ω intervals, of all the 194 studied AgNW networks in the *I-T* experiment. The red curve corresponds to a fitted Gaussian. The associated mean value μ of 13.4 Ω and standard deviation σ of 5.0 Ω are reported; **c)** Network resistance versus areal mass density (*amd*) of AgNW networks for the whole set of samples in the *I-T* experiment. The dashed line represents the power law (Eq. 3) between resistance and the network areal mass density. Inset represents a SEM picture of a network with a density of 73 ± 5 mg/m^2.

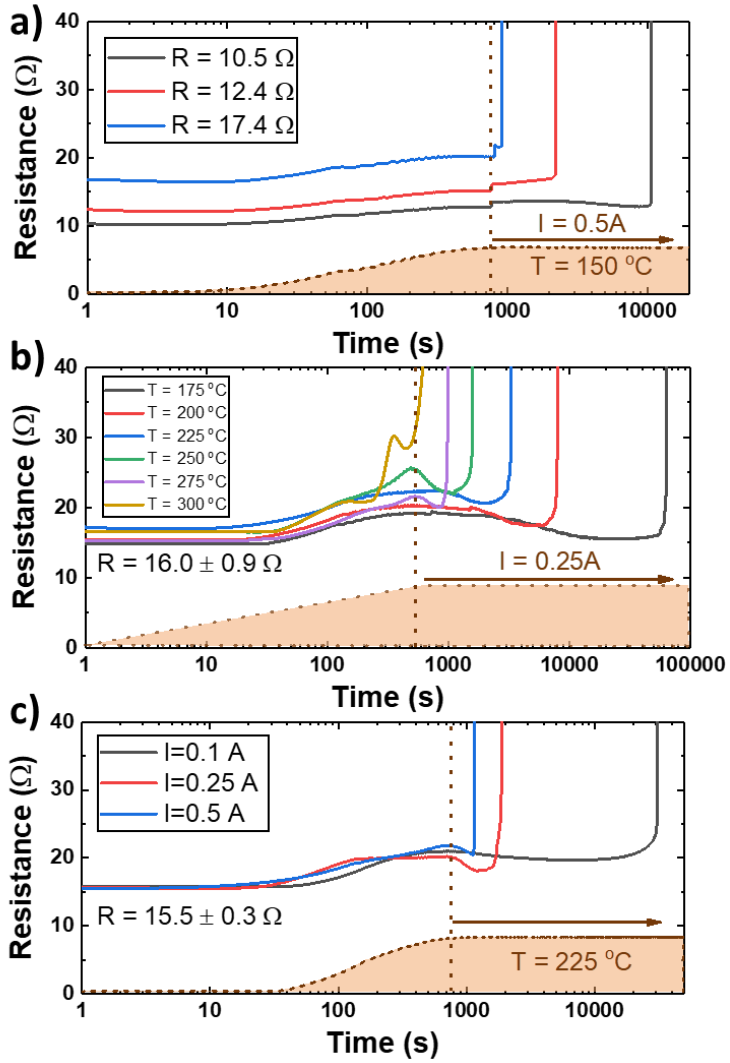

Figure 2. Influence of **a)** initial network resistance, **b)** applied temperature and **c)** applied current on the time of failure, depicted by the time evolution of resistance during the I-T experiment. In each case, the investigated parameter (initial resistance, current or temperature) is varied while the other two are maintained constant. The orange regions represent schematically the temperature evolution and the dashed vertical line shows the moment when the set temperature is reached and the current starts to be applied. **a)** Three samples with initial resistance from 10.5 to 17.4 Ω are tested under the 150 °C and a current of 0.5 A. **b)** Various temperatures from 175 to 300 °C are applied in a set of samples with similar resistance of 16.0 ± 0.9 Ω under constant current of 0.25 A. **c)** Three different values of current (0.1, 0.25, 0.5 A) are applied in a group of samples with similar resistance of 15.5 ± 0.3 Ω, at a temperature of 225 °C.

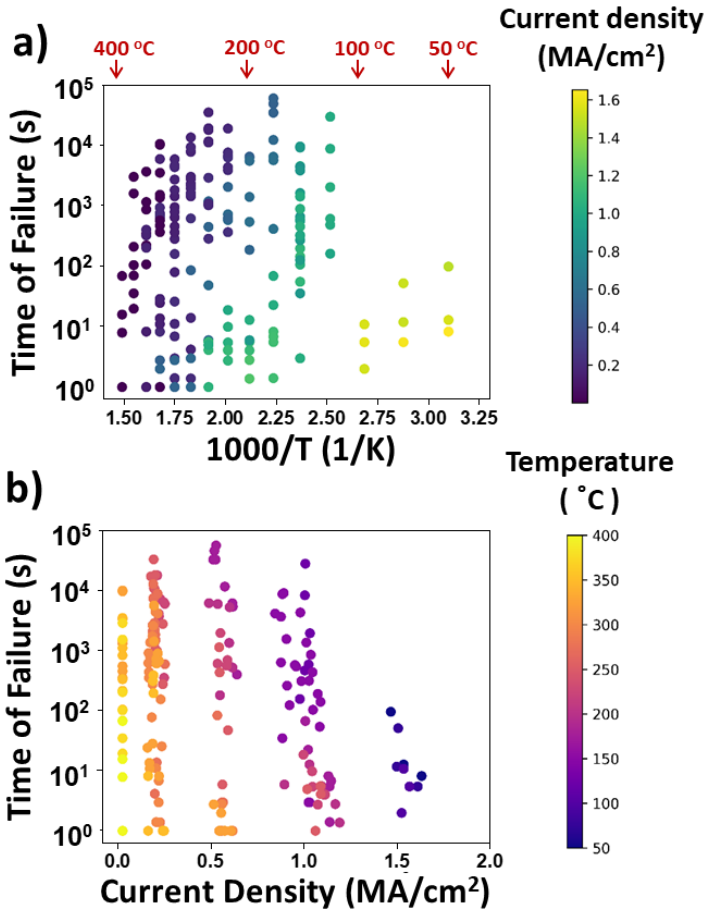

Figure 3. Time to failure associated to all AgNW networks of the *j-T* experiment plotted in log scale, with the current density calculated from the applied electrical bias and the initial resistance of each network. The graphs demonstrate the relation of *ToF* with **a)** the reciprocal temperature and **b)** the current density. The color scale of each data corresponds to the current density and the applied temperature, respectively.

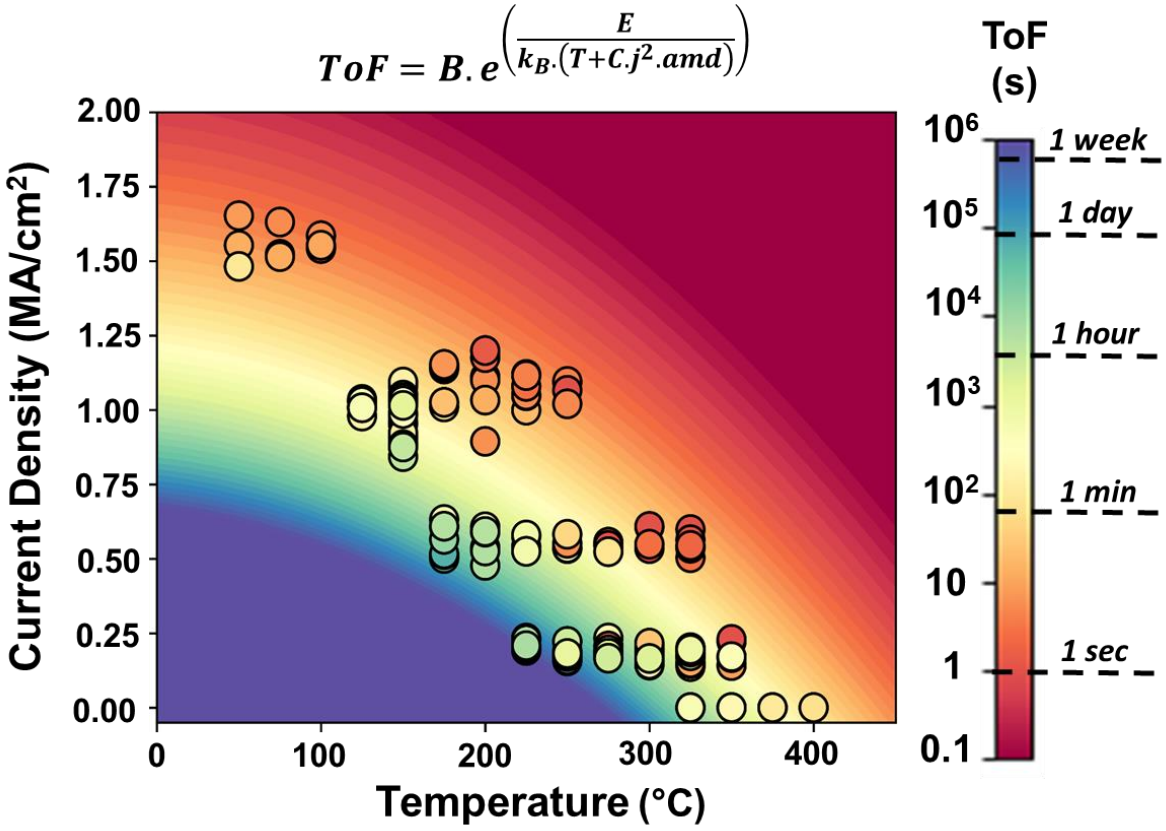

Figure 4. Current density - Temperature diagram (*j-T*) including both calculated and experimental values of the time of failure (*ToF*) for AgNW networks. The color map represents the calculated *ToF* and duration examples are noted in the rainbow scale, i.e. 1 second, 1 minute, 1 hour etc. The circles correspond to experimental *j-T* couples and their inside color corresponds to the experimentally measured *ToF*. The model equation is presented on top of the graph and corresponds to (Eq.13). The calculated *ToF* values correspond to a network electrical resistance of 13.4 Ω, associated to *amd* equal to 86 mg/m^2.

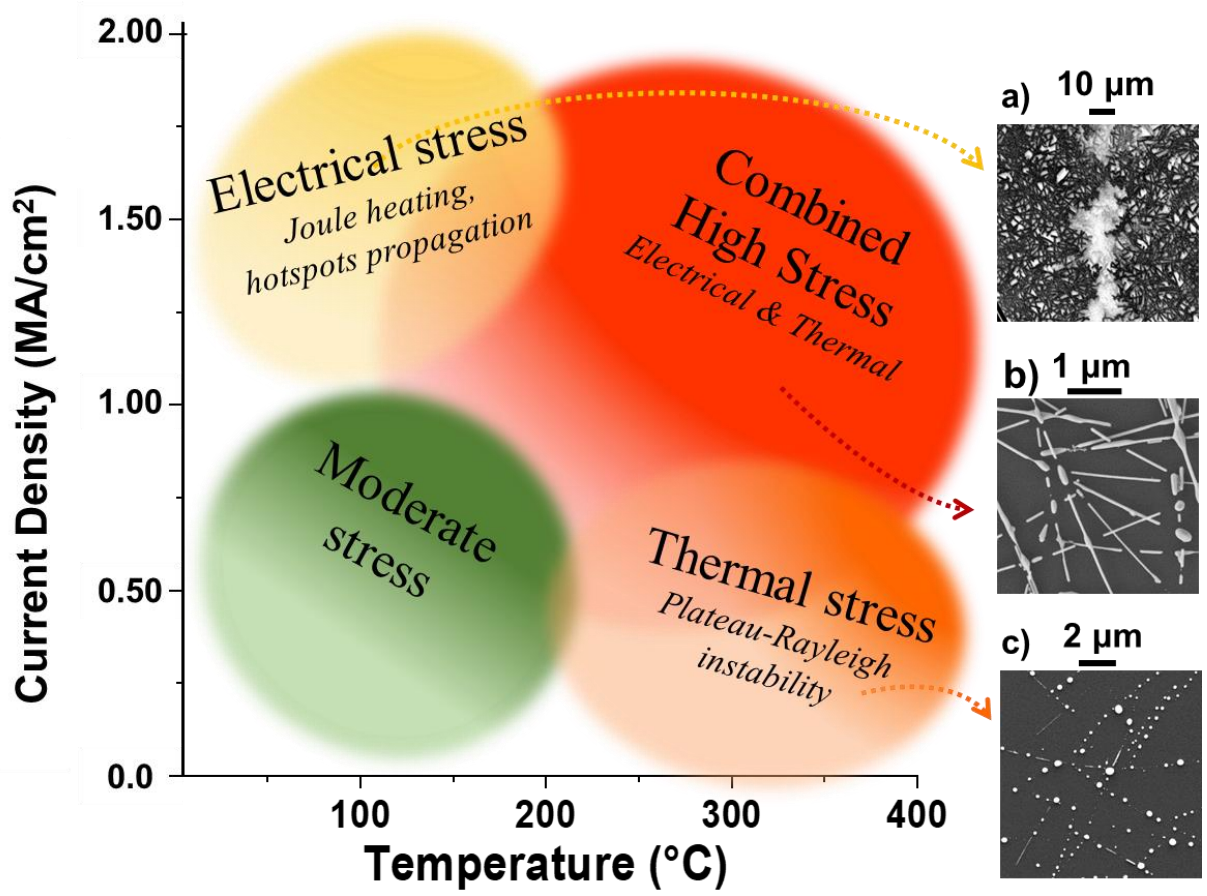

Figure 5. Schematic representation of the *j-T* experiment, showing the ranges of the applied current density and temperature. The extreme cases, where current density and/or temperature are high, lead to fast degradation of AgNWs and they are associated with different mechanisms of failure. SEM images correspond to the 3 general regimes of the degradation, when: **a)** solely a high current density is applied, i.e. 1.5 MA/cm^2, and the impact of the temperature is negligible (below 100 °C). In this case, the propagation of a crack has severely degraded AgNW within a very narrow area where the crack did propagate, **b)** high stress of both electrical and thermal nature is induced, with values above 1 MA/cm^2 and 200 °C, respectively; **c)** the thermal stress is dominant, with applied temperatures over 300 °C, and the current bias is roughly lower than 0.5 MA/cm^2. In this case, the Plateau-Rayleigh instability causes the spheroidization of the nanowires.

Table 1 Parameters determined in the *j-T* model and comparison with the literature

Parameters	Symbol	Units	Model Values	Literature Values	Reference
Thermal activation energy	E	eV	1.1 ± 0.1	0.3 - 1	Lagrange et al. [46]
Local heat transfer constant	α^{local}	$W.m^{-2}.K^{-1}$	96 ± 5	15-123	Sorel et al. [32]
Pre-factor diffusion coefficient	D_0	$m^2.s^{-1}$	(4.4 ±0.1) x 10^{-7}	3.7 x10^{-7}	Jamnig et al. [47]

TOC Graphical

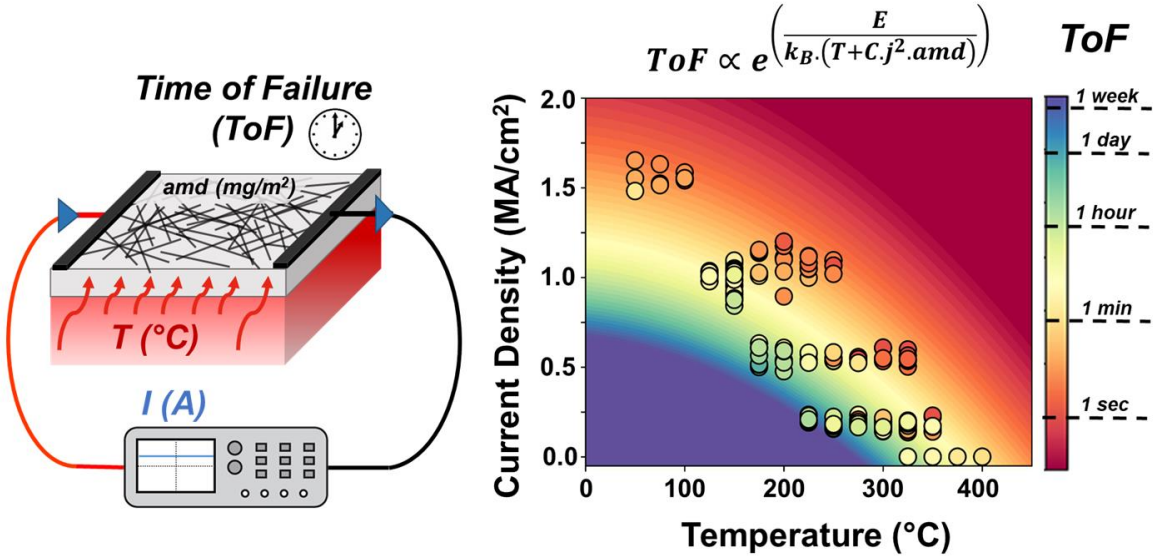

Acknowledgments

The authors would like to warmly thank Y. Bréchet, C. Celle, C. Mayousse, D.N. Nguyen and J.P. Simonato for fruitful discussions.

Associated Content

Supporting Information. In Supporting Information, the geometrical considerations are described to establish a cross section area (*CS*) dependence with the network areal mass density.

Author Information

Corresponding Author

*Corresponding authors: daniel.bellet@grenoble-inp.fr

Author Contributions

The manuscript was written through contributions of all authors. All authors have given approval to the final version of the manuscript. ‡These authors contributed equally.

Funding Sources

This work was funded by the Agence Nationale de Recherche (ANR, France) via the program ANR-18-CE09-0041 (Meaning) and ANR-18-CE09-0036 (Panassé).This work was also performed within the framework of the Centre of Excellence of Multifunctional Architectured Materials "CEMAM" n° AN-10-LABX-44-01. This work was as well supported by Région Auvergne Rhône-Alpes through the project Pack Ambition Recherche 2018 Eternité. This work was supported by LISBOA-05-3559-FSE-000007 and CENTRO-04-3559-FSE-000094

operations, co-funded by the Lisboa2020 ,Centro 2020 programme, Portugal 2020, European Union, through the European Social Fund, as well as by Fundação para a Ciência e Tecnologia (FCT) and Agência Nacional de Inovação (ANI).

References

(1) Langley, D.; Giusti, G.; Mayousse, C.; Celle, C.; Bellet, D.; Simonato, J.-P. Flexible Transparent Conductive Materials Based on Silver Nanowire Networks: A Review. *Nanotechnology* **2013**, *24* (45), 452001. https://doi.org/10.1088/0957-4484/24/45/452001.

(2) Sannicolo, T.; Lagrange, M.; Cabos, A.; Celle, C.; Simonato, J.-P.; Bellet, D. Metallic Nanowire-Based Transparent Electrodes for Next Generation Flexible Devices: A Review. *Small* **2016**, *12* (44), 6052–6075. https://doi.org/10.1002/smll.201602581.

(3) Papanastasiou, D. T.; Schultheiss, A.; Muñoz-Rojas, D.; Celle, C.; Carella, A.; Simonato, J.-P.; Bellet, D. Transparent Heaters: A Review. *Advanced Functional Materials* **2020**, 1910225. https://doi.org/10.1002/adfm.201910225.

(4) Ellmer, K. Past Achievements and Future Challenges in the Development of Optically Transparent Electrodes. *Nature Photonics* **2012**, *6* (12), 809–817. https://doi.org/10.1038/nphoton.2012.282.

(5) Jung, J.; Lee, H.; Ha, I.; Cho, H.; Kim, K. K.; Kwon, J.; Won, P.; Hong, S.; Ko, S. H. Highly Stretchable and Transparent Electromagnetic Interference Shielding Film Based on Silver Nanowire Percolation Network for Wearable Electronics Applications. *ACS Appl. Mater. Interfaces* **2017**, *9* (51), 44609–44616. https://doi.org/10.1021/acsami.7b14626.

(6) Wang, J.-L.; Lu, Y.-R.; Li, H.-H.; Liu, J.-W.; Yu, S.-H. Large Area Co-Assembly of Nanowires for Flexible Transparent Smart Windows. *J. Am. Chem. Soc.* **2017**, *139* (29), 9921–9926. https://doi.org/10.1021/jacs.7b03227.

(7) Resende, J.; Sekkat, A.; Nguyen, V. H.; Chatin, T.; Jiménez, C.; Burriel, M.; Bellet, D.; Muñoz-Rojas, D. Planar and Transparent Memristive Devices Based on Titanium Oxide Coated Silver Nanowire Networks with Tunable Switching Voltage. *Small* **2021**, *17* (21), 2007344. https://doi.org/10.1002/smll.202007344.

(8) Polat Genlik, S.; Tigan, D.; Kocak, Y.; Ercan, K. E.; Cicek, M. O.; Tunca, S.; Koylan, S.; Coskun, S.; Ozensoy, E.; Unalan, H. E. All-Solution-Processed, Oxidation-Resistant Copper Nanowire Networks for Optoelectronic Applications with Year-Long Stability. *ACS*

Appl. Mater. Interfaces **2020**, *12* (40), 45136–45144. https://doi.org/10.1021/acsami.0c11729.

(9) Bang, J.; Coskun, S.; Pyun, K. R.; Doganay, D.; Tunca, S.; Koylan, S.; Kim, D.; Unalan, H. E.; Ko, S. H. Advances in Protective Layer-Coating on Metal Nanowires with Enhanced Stability and Their Applications. *Applied Materials Today* **2021**, *22*, 100909. https://doi.org/10.1016/j.apmt.2020.100909.

(10) Martin Lokan; Roderick Eggert; Michael Redlinger. *The Availability of Indium: The Present, Medium Term, and Long Term*; NREL-Colorado School of Mines, 2015; p 79.

(11) Nguyen, V. H.; Resende, J.; Papanastasiou, D. T.; Fontanals, N.; Jiménez, C.; Muñoz-Rojas, D.; Bellet, D. Low-Cost Fabrication of Flexible Transparent Electrodes Based on Al Doped ZnO and Silver Nanowire Nanocomposites: Impact of the Network Density. *Nanoscale* **2019**, *11* (25), 12097–12107. https://doi.org/10.1039/C9NR02664A.

(12) McLellan, K.; Yoon, Y.; Leung, S. N.; Ko, S. H. Recent Progress in Transparent Conductors Based on Nanomaterials: Advancements and Challenges. *Adv. Mater. Technol.* **2020**, *5* (4), 1900939. https://doi.org/10.1002/admt.201900939.

(13) Azani, M.; Hassanpour, A.; Torres, T. Benefits, Problems, and Solutions of Silver Nanowire Transparent Conductive Electrodes in Indium Tin Oxide (ITO)-Free Flexible Solar Cells. *Adv. Energy Mater.* **2020**, 2002536. https://doi.org/10.1002/aenm.202002536.

(14) Lagrange, M.; Langley, D. P.; Giusti, G.; Jiménez, C.; Bréchet, Y.; Bellet, D. Optimization of Silver Nanowire-Based Transparent Electrodes: Effects of Density, Size and Thermal Annealing. *Nanoscale* **2015**, *7* (41), 17410–17423. https://doi.org/10.1039/C5NR04084A.

(15) Bellet, D.; Lagrange, M.; Sannicolo, T.; Aghazadehchors, S.; Nguyen, V. H.; Langley, D. P.; Muñoz-Rojas, D.; Jiménez, C.; Bréchet, Y.; Nguyen, N. D. Transparent Electrodes Based on Silver Nanowire Networks: From Physical Considerations towards Device Integration. *Materials* **2017**, *10* (6), 570. https://doi.org/10.3390/ma10060570.

(16) Jia, G.; Plentz, J.; Dellith, A.; Schmidt, C.; Dellith, J.; Schmidl, G.; Andrä, G. Biomimic Vein-Like Transparent Conducting Electrodes with Low Sheet Resistance and Metal Consumption. *Nano-Micro Lett.* **2020**, *12* (1), 19. https://doi.org/10.1007/s40820-019-0359-9.

(17) Li, W.; Zhang, H.; Shi, S.; Xu, J.; Qin, X.; He, Q.; Yang, K.; Dai, W.; Liu, G.; Zhou, Q.; Yu, H.; Silva, S. R. P.; Fahlman, M. Recent Progress in Silver Nanowire Networks for Flexible Organic Electronics. *J. Mater. Chem. C* **2020**, *8* (14), 4636–4674. https://doi.org/10.1039/C9TC06865A.

(18) Langley, D. P.; Lagrange, M.; Giusti, G.; Jiménez, C.; Bréchet, Y.; Nguyen, N. D.; Bellet, D. Metallic Nanowire Networks: Effects of Thermal Annealing on Electrical Resistance. *Nanoscale* **2014**, *6*, 13535–13543. https://doi.org/10.1039/C4NR04151H.

(19) Wang, J.; Jiu, J.; Araki, T.; Nogi, M.; Sugahara, T.; Nagao, S.; Koga, H.; He, P.; Suganuma, K. Silver Nanowire Electrodes: Conductivity Improvement Without Post-Treatment and Application in Capacitive Pressure Sensors. *Nano-Micro Lett.* **2015**, *7* (1), 51–58. https://doi.org/10.1007/s40820-014-0018-0.

(20) Vafaei, A.; Hu, A.; Goldthorpe, I. A. Joining of Individual Silver Nanowires via Electrical Current. *Nano-Micro Letters* **2014**, *6* (4), 293–300. https://doi.org/10.1007/s40820-014-0001-9.

(21) Tokuno, T.; Nogi, M.; Karakawa, M.; Jiu, J.; Nge, T. T.; Aso, Y.; Suganuma, K. Fabrication of Silver Nanowire Transparent Electrodes at Room Temperature. *Nano Research* **2011**, *4* (12), 1215–1222. https://doi.org/10.1007/s12274-011-0172-3.

(22) Park, J. H.; Hwang, G.-T.; Kim, S.; Seo, J.; Park, H.-J.; Yu, K.; Kim, T.-S.; Lee, K. J. Flash-Induced Self-Limited Plasmonic Welding of Silver Nanowire Network for Transparent Flexible Energy Harvester. *Advanced Materials* **2017**, *29* (5), 1603473. https://doi.org/10.1002/adma.201603473.

(23) Liu, L.; Li, H.-Y.; Ye, D.; Yu, Y.; Liu, L.; Wu, Y. Nanowelding and Patterning of Silver Nanowires via Mask-Free Atmospheric Cold Plasma-Jet Scanning. *Nanotechnology* **2017**, *28* (22), 225301. https://doi.org/10.1088/1361-6528/aa6dd6.

(24) Xue, Z.; Xu, M.; Zhao, Y.; Wang, J.; Jiang, X.; Yu, L.; Wang, J.; Xu, J.; Shi, Y.; Chen, K.; Cabarrocas, P. R. i. Engineering Island-Chain Silicon Nanowires via a Droplet Mediated Plateau-Rayleigh Transformation. *Nature Communications* **2016**, *7*, ncomms12836. https://doi.org/10.1038/ncomms12836.

(25) de Gennes, P.-G.; Brochard-Wyart, F.; Quéré, D. *Capillarity and Wetting Phenomena - Drops, Bubbles, Pearls, Waves*; Springer New York, 2004.

(26) Karim, S.; Toimil-Molares, M. E.; Balogh, A. G.; Ensinger, W.; Cornelius, T. W.; Khan, E. U.; Neumann, R. Morphological Evolution of Au Nanowires Controlled by Rayleigh Instability. *Nanotechnology* **2006**, *17* (24), 5954–5959. https://doi.org/10.1088/0957-4484/17/24/009.

(27) Toimil Molares, M. E.; Balogh, A. G.; Cornelius, T. W.; Neumann, R.; Trautmann, C. Fragmentation of Nanowires Driven by Rayleigh Instability. *Applied Physics Letters* **2004**, *85* (22), 5337–5339. https://doi.org/doi:10.1063/1.1826237.

(28) Gill, S. P. A. Controlling the Rayleigh Instability of Nanowires. *Appl. Phys. Lett.* **2013**, *102* (14), 143108. https://doi.org/10.1063/1.4801766.

(29) Patil, J. J.; Chae, W. H.; Trebach, A.; Carter, K.; Lee, E.; Sannicolo, T.; Grossman, J. C. Failing Forward: Stability of Transparent Electrodes Based on Metal Nanowire Networks. *Adv. Mater.* **2020**, 2004356. https://doi.org/10.1002/adma.202004356.

(30) Khaligh, H. H.; Goldthorpe, I. A. Failure of Silver Nanowire Transparent Electrodes under Current Flow. *Nanoscale Research Letters* **2013**, *8* (1), 235. https://doi.org/10.1186/1556-276X-8-235.

(31) Mayousse, C.; Celle, C.; Fraczkiewicz, A.; Simonato, J.-P. Stability of Silver Nanowire Based Electrodes under Environmental and Electrical Stresses. *Nanoscale* **2015**, *7* (5), 2107–2115. https://doi.org/10.1039/C4NR06783E.

(32) Sorel, S.; Bellet, D.; Coleman, J. N. Relationship between Material Properties and Transparent Heater Performance for Both Bulk-like and Percolative Nanostructured Networks. *ACS Nano* **2014**, *8* (5), 4805–4814. https://doi.org/10.1021/nn500692d.

(33) Sannicolo, T.; Charvin, N.; Flandin, L.; Kraus, S.; Papanastasiou, D. T.; Celle, C.; Simonato, J.-P.; Muñoz-Rojas, D.; Jiménez, C.; Bellet, D. Electrical Mapping of Silver Nanowire Networks: A Versatile Tool for Imaging Network Homogeneity and Degradation Dynamics during Failure. *ACS Nano* **2018**, *12* (5), 4648–4659. https://doi.org/10.1021/acsnano.8b01242.

(34) Wang, K.; Jin, Y.; Wang, X.; Qian, B.; Wang, J.; Xiao, F. Investigation into the Failure Mechanism of Silver Nanowire Network Film under Electrical Stress. In *2020 IEEE 70th Electronic Components and Technology Conference (ECTC)*; IEEE: Orlando, FL, USA, 2020; pp 1218–1224. https://doi.org/10.1109/ECTC32862.2020.00195.

(35) Wang, K.; Jin, Y.; Xiao, F. Long-Term Electrically Stable Silver Nanowire Composite Transparent Electrode under High Current Density. *J Mater Sci: Mater Electron* **2021**. https://doi.org/10.1007/s10854-021-06386-4.

(36) Charvin, N.; Resende, J.; Papanastasiou, D. T.; Muñoz-Rojas, D.; Jiménez, C.; Nourdine, A.; Bellet, D.; Flandin, L. Dynamic Degradation of Metallic Nanowire Networks under Electrical Stress: A Comparison between Experiments and Simulations. *Nanoscale Adv.* **2021**, *3* (3), 675–681. https://doi.org/10.1039/D0NA00895H.

(37) Bardet, L.; Papanastasiou, D. T.; Crivello, C.; Akbari, M.; Resende, J.; Sekkat, A.; Sanchez-Velasquez, C.; Rapenne, L.; Jiménez, C.; Muñoz-Rojas, D.; Denneulin, A.; Bellet, D. Silver Nanowire Networks: Ways to Enhance Their Physical Properties and Stability. *Nanomaterials* **2021**, *11* (11), 2785. https://doi.org/10.3390/nano11112785.

(38) De, S.; Coleman, J. N. The Effects of Percolation in Nanostructured Transparent Conductors. *MRS Bulletin* **2011**, *36* (10), 774–781. https://doi.org/10.1557/mrs.2011.236.

(39) Sannicolo, T.; Muñoz-Rojas, D.; Nguyen, N. D.; Moreau, S.; Celle, C.; Simonato, J.-P.; Bréchet, Y.; Bellet, D. Direct Imaging of the Onset of Electrical Conduction in Silver Nanowire Networks by Infrared Thermography: Evidence of Geometrical Quantized Percolation. *Nano Letters* **2016**, *16* (11), 7046–7053. https://doi.org/10.1021/acs.nanolett.6b03270.

(40) Philibert, J. *Atom Movements: Diffusion and Mass Transport in Solids*; Monographies de physique; Editions de Physique: Les Ulis, France, 1991.

(41) Lagrange, M.; Sannicolo, T.; Muñoz-Rojas, D.; Lohan, B. G.; Khan, A.; Anikin, M.; Jiménez, C.; Bruckert, F.; Bréchet, Y.; D Bellet. Understanding the Mechanisms Leading to Failure in Metallic Nanowire-Based Transparent Heaters, and Solution for Stability Enhancement. *Nanotechnology* **2017**, *28* (5), 055709. https://doi.org/10.1088/1361-6528/28/5/055709.

(42) Khaligh, H. H.; Xu, L.; Khosropour, A.; Madeira, A.; Romano, M.; Pradére, C.; Tréguer-Delapierre, M.; Servant, L.; Pope, M. A.; Goldthorpe, I. A. The Joule Heating Problem in Silver Nanowire Transparent Electrodes. *Nanotechnology* **2017**, *28* (42), 425703. https://doi.org/10.1088/1361-6528/aa7f34.

(43) Bid, A.; Bora, A.; Raychaudhuri, A. K. Temperature Dependence of the Resistance of Metallic Nanowires of Diameter ≥ 15 Nm: Applicability of Bloch-Grüneisen Theorem. *Phys. Rev. B* **2006**, *74* (3), 035426. https://doi.org/10.1103/PhysRevB.74.035426.

(44) Mayousse, C.; Celle, C.; Moreau, E.; Mainguet, J.-F.; Carella, A.; Simonato, J.-P. Improvements in Purification of Silver Nanowires by Decantation and Fabrication of Flexible Transparent Electrodes. Application to Capacitive Touch Sensors. *Nanotechnology* **2013**, *24* (21), 215501.

(45) Madeira, A.; Papanastasiou, D. T.; Toupance, T.; Servant, L.; Tréguer-Delapierre, M.; Bellet, D.; Goldthorpe, I. A. Rapid Synthesis of Ultra-Long Silver Nanowires for High Performance Transparent Electrodes. *Nanoscale Adv.* **2020**, *2* (9), 3804–3808. https://doi.org/10.1039/D0NA00392A.

(46) Lagrange, M. Physical Analysis of Percolating Silver Nanowire Networks Used as Transparent Electrodes for Flexible Applications. PhD thesis, University of Grenoble Alpes (France), 2015.

(47) Jamnig, A.; Sangiovanni, D. G.; Abadias, G.; Sarakinos, K. Atomic-Scale Diffusion Rates during Growth of Thin Metal Films on Weakly-Interacting Substrates. *Sci Rep* **2019**, *9* (1), 6640. https://doi.org/10.1038/s41598-019-43107-8.

(48) Black, J. R. Electromigration—A Brief Survey and Some Recent Results. *IEEE Transactions on Electron Devices* **1969**, *16* (4), 338–347. https://doi.org/10.1109/T-ED.1969.16754.

(49) Stahlmecke, B.; Meyer zu Heringdorf, F.-J.; Chelaru, L. I.; Horn-von Hoegen, M.; Dumpich, G.; Roos, K. R. Electromigration in Self-Organized Single-Crystalline Silver Nanowires. *Applied Physics Letters* **2006**, *88* (5), 053122. https://doi.org/10.1063/1.2172012.

(50) Khan, A.; Nguyen, V. H.; Muñoz-Rojas, D.; Aghazadehchors, S.; Jiménez, C.; Nguyen, N. D.; Bellet, D. Stability Enhancement of Silver Nanowire Networks with Conformal ZnO

Coatings Deposited by Atmospheric Pressure Spatial Atomic Layer Deposition. *ACS Applied Materials & Interfaces* **2018**, *10* (22), 19208–19217. https://doi.org/10.1021/acsami.8b03079.

(51) Muñoz-Rojas, D.; Nguyen, V. H.; Masse de la Huerta, C.; Aghazadehchors, S.; Jiménez, C.; Bellet, D. Spatial Atomic Layer Deposition (SALD), an Emerging Tool for Energy Materials. Application to New-Generation Photovoltaic Devices and Transparent Conductive Materials. *Comptes Rendus Physique* **2017**, *18* (7), 391–400. https://doi.org/10.1016/j.crhy.2017.09.004.

(52) Mayousse, C.; Celle, C.; Moreau, E.; Mainguet, J.-F.; Carella, A.; Simonato, J.-P. Improvements in Purification of Silver Nanowires by Decantation and Fabrication of Flexible Transparent Electrodes. Application to Capacitive Touch Sensors. *Nanotechnology* **2013**, *24* (21), 215501. https://doi.org/10.1088/0957-4484/24/21/215501.